Title

A Synchronized Lissajous-based Method to Detect and Classify Events in Synchro-waveform Measurements in Power Distribution Networks

Authors

Izadi, Milad
Mohsenian-Rad, Hamed

Publication Date

2022-02-03

Peer reviewed

A Synchronized Lissajous-based Method to Detect and Classify Events in Synchro-waveform Measurements in Power Distribution Networks

Milad Izadi, *Student Member, IEEE* and Hamed Mohsenian-Rad, *Fellow, IEEE*

***Abstract*—Waveform measurement units (WMUs) are a new class of smart grid sensors. They capture *synchro-waveforms*, i.e., time-synchronized high-resolution voltage waveform and current waveform measurements. In this paper, we propose new methods to *detect* and *classify* power quality events in power distribution systems by using synchro-waveform measurements. The methods are built upon a novel graphical concept, called *synchronized Lissajous curve*. The proposed event detection and event classification methods work by analyzing the *shape* of the synchronized Lissajous curves during disturbances and events. The impact of challenging factors, such as the angle, the location, and other parameters of the event are discussed. We show that these challenges can be addressed if we treat the synchronized Lissajous curves as *images*, instead of as time series as in the raw synchronized waveform measurements. Hence, we can take advantage of the recent advancements in the field of *image processing* so as to capture the overall characterizing patterns in the shapes of the synchronized Lissajous curves. We develop a Convolutional Neural Network (CNN) method to classify the events, where the input is the synchronized Lissajous images. The effectiveness of the proposed event detection and classification methods is demonstrated through computer simulations, including hardware-in-the-loop simulations, and real-world field data. Multiple case studies verify the performance of the proposed methods. The proposed event detection method can accurately detect events, and identify the start time and the end time of each event. The proposed event classification method can classify power quality events with high accuracy. The proposed detection and classification methods do *not* require any prior knowledge about the network. They use data from as few as *only two* WMUs.**

***Index Terms*—Synchro-waveform, data-driven method, waveform measurement unit, power quality event, convolutional neural network, synchronized Lissajous curves, detection, classification, image classification, hardware-in-the-loop simulations.**

I. Introduction

WAVEFORM measurement units (WMUs) are a new class of smart grid sensors that provide precise time-synchronized voltage and current waveform measurements in time domain [1]–[9]. The very high reporting rate of WMUs, such as 256 samples per cycle, and the fact we have access to synchronized waveform measurements, can significantly enhance situational awareness and operational intelligence in power distribution networks [8], [9]. So far, WMUs have been used in only a few number of applications, such as to study harmonics in transformers [1] or to identify the source location of power quality events [2] and incipient faults [3].

It is worth clarifying that the term WMU is relatively new. While phasor measurement units (PMUs) are used to measure *synchro-phasors* [10], WMUs are used to measure *synchro-waveforms* [3], [11], [12]. The term WMU is gradually starting to appear in the academic literature, e.g., see [2], [7], and also in the industry reports, e.g., see [13], [14]. Given the much higher reporting rate of WMUs than PMUs, and also because WMUs have much less internal filtering than PMUs, WMUs are capable of capturing several details about the voltage waveforms and current waveforms that are inherently impossible for PMUs to capture. Illustrative examples on the details that *can* be captured by WMUs but *cannot* be captured by PMUs are available in Section I-A in [3].

In this paper, we seek to propose a novel data-driven situational awareness framework based on a fundamentally new graphical concept, called *synchronized Lissajous curve*, in power distribution systems. The synchronized Lissajous curve is obtained by plotting the difference of two synchronized voltage waveforms versus the difference of two synchronized current waveforms. Our goal is to use the synchronized Lissajous-based representation of the WMU measurements to accurately detect and classify various power quality events.

A. Summary of Technical Contributions

The main contributions in this paper are as follows:

1) A new data-driven situational awareness framework is proposed in power distribution systems based on the analysis of synchro-waveform measurements. The new framework is built upon the new concept of synchronized Lissajous curves. During normal operating conditions, the synchronized Lissajous curve is an ellipse. Once an event or a disturbance occurs, the *shape* and the *area* of the synchronized Lissajous curve can change significantly, depending on the type, location, and other characteristics of the event.
2) The proposed event detection method monitors the changes in the areas of two successive synchronized Lissajous curves. Once an event occurs, the area sharply changes, indicating that an event has occurred. We present an adaptive detection threshold based on a statistical threshold selection method that is robust against outliers.
3) The proposed event classification method works by classifying the synchronized Lissajous *images*. A Convolutional Neural Network (CNN) is developed as the image classification method. Our approach is in sharp contrast to the common practice in the literature to conduct classification based on the time series of the waveform measurements. The proposed classification method reaches a high accuracy, even at lower measurement reporting rates, under missing data, and under major measurement noise.

The authors are with the University of California, Riverside, CA, USA; e-mails: {mizadi, hamed}@ece.ucr.edu. This work was supported in part by UCOP grant LFR-18-548175. The corresponding author is H. Mohsenian-Rad.

4) The proposed framework is able to correctly detect and classify a wide range of events, such as sustained events with steady-state component, e.g., high impedance fault; sustained events with transient component, e.g., capacitor bank switching; and temporary events with very short duration, e.g., incipient faults. The proposed detection and classification methods are model-free and they do *not* require any knowledge about the network. These methods require data from as few as only two WMUs.

B. Related Literature

The topic of synchro-waveform measurements is new and the related literature is starting to emerge only recently. The basic ideas and comparison with supervisory control and data acquisition (SCADA) measurements and PMU measurements are discussed in [1]. Methods based on modal analysis at damping frequencies are presented in [2], [3] to identify the location of power quality events and incipient faults using synchro-waveform measurements. A analysis based on eliminating the fundamental frequency component is done in [15] to identify sub-synchronous resonance.

Importantly, for a method to be truly relevant to synchro-waveform measurements, it must take advantage of the *synchronized* waveform measurements from *multiple* WMUs. However, even before the development of synchro-waveforms, there was a literature on the analysis of waveform measurements that come from *individual* power quality sensors. Both event detection and event classification are addressed in such literature; but the focus has been mainly on major events such as major faults.

Traditionally, a common approach in event detection has been to monitor the changes in the root-mean-square (RMS) of the voltage waveforms, e.g., in [16]. There are other methods that work based on signal processing tools, such as wavelet transform [17], wavelet packet transform [18], S-transform [19], and Fourier transform [20]. Although these methods perform well in many cases, they are often sensitive to the presence of harmonics in the waveforms and also to the parameters of the transformation technique that is being used. Unlike the above and other similar methods, the event detection method in this paper is meant for *synchro-waveform* measurements as it takes direct advantage of the multiple available synchronized waveform measurements. It works in time-domain therefore it does not require any data transformation. It is not sensitive to harmonics. Furthermore, it makes use of both the synchronized voltage waveform and the current waveform measurements.

As for the traditional methods on event classification, various techniques have been used, such as decision trees [21], neural networks [22], support vector machines [23], and hierarchical process [24]. The common approach in the above papers and other similar studies is to conduct event classification based on the *time series* data that come from power quality sensors. In a sharp contract, here we propose a fundamentally different approach to conduct event classification based on the graphical representation of the events in Lissajous images. Accordingly, our method is a CNN-based image classification. It is designed to use both the synchronized voltage waveform measurements and the synchronized current waveform measurements.

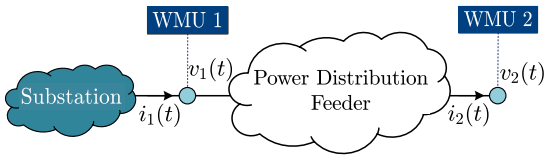

Fig. 1. A distribution feeder that is equipped with two WMUs.

There is a limited literature on classifying power quality events using image classification methods, including different choices of CNN models. For example, in [25]–[27], wavelet transformation is used to generate *scalogram* image representation for the power quality events. As another example, in [28], image representation of the waveforms is done by using the *space-phasor* analysis and discrete quantization. To the best of our knowledge, no prior study has used any variation of the synchronized Lissajous curves to conduct event classification in this context. Furthermore, all the prior studies are focused on making use of only event classification based on measurements from only one power quality or waveform sensor.

We introduced the concept of synchronized Lissajous curves for the first time in the preliminary conference version of this paper in [8]; where we discussed the potential use of such curves in achieving situational awareness. The focus was on showing illustrative examples to present events based on the synchronized Lissajous curves. We have also recently identified different variations of synchronized Lissajous curves and their basic characteristics in a letter paper in [9]. In this paper, we develop the actual methods to achieve event detection and event classification using synchronized Lissajous curves.

II. Cyclic Synchronized Lissajous Curve Representation of a Power Quality Event

Consider a power distribution feeder, such as the one in Fig. 1. Suppose two WMUs are installed on this feeder, where WMU 1 is installed at the beginning of the feeder and WMU 2 is installed at the end of the feeder. Let $v_1(t)$ denote the voltage waveform and $i_1(t)$ denote the current waveform that are measured by WMU 1. Also, let $v_2(t)$ denote the voltage waveform and $i_2(t)$ denote the current waveform that are measured by WMU 2. The waveform measurements are time-synchronized. When an event occurs somewhere on the power distribution feeder, it creates signatures in the waveform measurements that are captured by both WMUs 1 and 2. In this regard, we define the following two new waveforms [8], [9]:

$$v(t) = v_1(t) - v_2(t), \tag{1}$$

$$i(t) = i_1(t) - i_2(t). \tag{2}$$

The waveform in (1) is the *difference* between the voltage waveforms at WMU 1 and WMU 2. The waveform in (2) is the *difference* between the current waveforms at WMU 1 and WMU 2. If WMU 1 and WMU 2 are not in the same nominal voltage levels, then we can define (1) and (2) in per unit.

Figs. 2(a) and (b) show examples of the synchronized wavefoms in (1) and (2) that are captured by WMUs 1 and 2 when a power quality disturbance occurs. The impact of the disturbance is clearly visible in these synchronized waveforms.

A. Synchronized Lissajous Curve

The waveform measurements in (1) and (2) can be graphically represented as a Lissajous curve. A Lissajous curve is a graph that is constructed by plotting one waveform versus another waveform. It has various applications in signal and image processing; such as in electrocardiogram analysis and dielectric discharge analysis [29]. Furthermore, the Lissajous curves have had occasional applications also in power system engineering; such as to analyze non-linear single-phase circuits [30] or to identify fault location in transmission lines [31]. However, these existing applications have focused on the specific physical characteristics of the particular circuit or the particular equipment of interest.

In this paper, we propose to plot the voltage waveform *difference* in (1) versus the current waveform *difference* in (2). We refer to such Lissajous curve as the *synchronized Lissajous curve* [8], [9]; because it is constructed based on synchronized waveform measurements in WMU 1 and WMU 2.

The synchronized Lissajous curve that is corresponding to the waveforms in Fig. 2(a) and (b) is shown in Fig. 2(c). The blue curve represents the *pre-disturbance* conditions, i.e., the normal operating conditions before the disturbance occurs. The red curve represents the *post-disturbance* conditions, i.e., the circumstances immediately after the disturbance occurs.

The basic characteristics of the synchronized Lissajous curves have been derived in our recent work in [9]. Here, we briefly summarize them. First, as shown in Section IV-A in [9], the *area* of the synchronized Lissajous curve that is used in this paper can be interpreted as the weighted summation of the reactive power that one can define with respect to the voltage waveform in (1) and the current waveform in (2). It is worth adding that, there exists another definition for the synchronized Lissajous curve whose area can be interpreted as the weighted summation of the active power that one can define with respect to the voltage waveform in (1) and the current waveform in (2). Second, as shown in Section IV-B in [9], the *rotational angle* of the synchronized Lissajous curve provides insights about the location of the event. The rotational angle can also be interpreted as the impedance of the feeder as seen by the two WMUs. Third, as shown in Section IV-C in [9], the *shape* of the synchronized Lissajous curve is very informative about the cause of the event. In the absence of an event, i.e., during normal operation conditions, the shape of the synchronized Lissajous curves is proven to be an *ellipse*, see its proof in Section IV-C in [9]. However, once an event occurs, the synchronized Lissajous curve can take different shapes depending on the nature of the event. For example, in Fig. 2(c), the pre-disturbance curve is an ellipse (in blue); while the post-disturbance curve is a very different shape (in red).

Inspired by the above basic characteristics, in this paper, we develop new data-driven algorithms to utilize the synchronized Lissajous curves for event detection and event classification.

B. Different Shapes of Power Quality Events

Once an event occurs, the synchronized Lissajous curve deviates from its initial ellipse shape. The new (i.e., post-event) shape of the synchronized Lissajous curve would depend on the type of the event. To better understand the pre-disturbance and post-disturbance conditions, it is beneficial to plot the synchronized Lissajous curve *separately for each cycle*. Such sequence of the graphical snapshots can be referred to as *cyclic* synchronized Lissajous curve. Fig. 3 shows five successive cycles of the synchronized Lissajous curves for three different power quality events, respectively. In all three cases, the cyclic synchronized Lissajous curves are initially an ellipse but then they change to some other shapes.

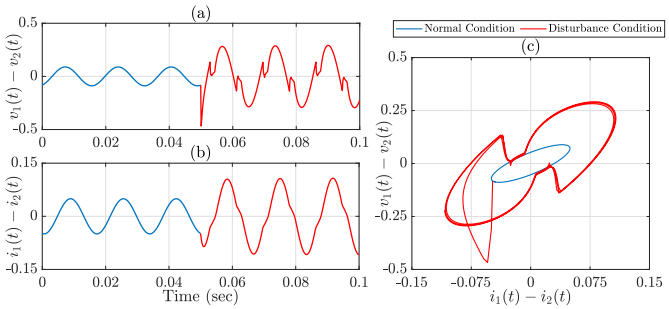

Fig. 2. An example of the synchronized Lissajous curve for a high impedance fault on a distribution feeder that is seen by two WMUs during normal operating conditions (blue) and disturbance conditions (red) [8]: (a) the difference of two synchronized voltage waveform; (b) the difference of two synchronized current waveform measurements; (c) the corresponding synchronized Lissajous curve.

We can distinguish two broad types of disturbances: *sustained disturbances*; such as high impedance faults and capacitor bank switching; and *temporary disturbances*, such as incipient faults. For the events in Fig. 3, the first and the second events are sustained while the third event is only temporary.

As shown in Figs. 3(a)-(e), if a high impedance fault occurs, the synchronized Lissajous curve deviates to a very different shape, see Figs. 3(c)-(e), compared with the ellipse shape during the normal operating condition, see Figs. 3(a)-(b). This is because the fault current in the high impedance fault contains odd order harmonics. As shown in Figs. 3(f)-(j), if a capacitor bank switches on, then the synchronized Lissajous curve oscillates for a very short period of time and then it converges to a new (different) ellipse shape, see Figs. 3(h)-(i). This happens because of the new transient mode of oscillation of the capacitor bank [2], [3]. As shown in Figs. 3(k)-(o), if an incipient fault occurs, then the synchronized Lissajous curve deviates from the shape of an ellipse for the duration of the incipient fault, see Figs. 3(m)-(n), then it turns back to the ellipse shape at the normal operating condition, see Fig. 3(o). This happens because the incipient fault is self-clearing and has a very short duration.

The above examples show that the shape of the synchronized Lissajous curve can draw a unique picture about the presence and the root cause of the power quality events.

C. Intuition based on Circuit Analysis

Even though the analysis in this paper is data-driven, one can still discuss the event-triggered changes in synchronized Lissajous curves also in the context of the underlying power distribution circuit. Such analysis can provide additional insights on why it is reasonable to use the voltage waveform in

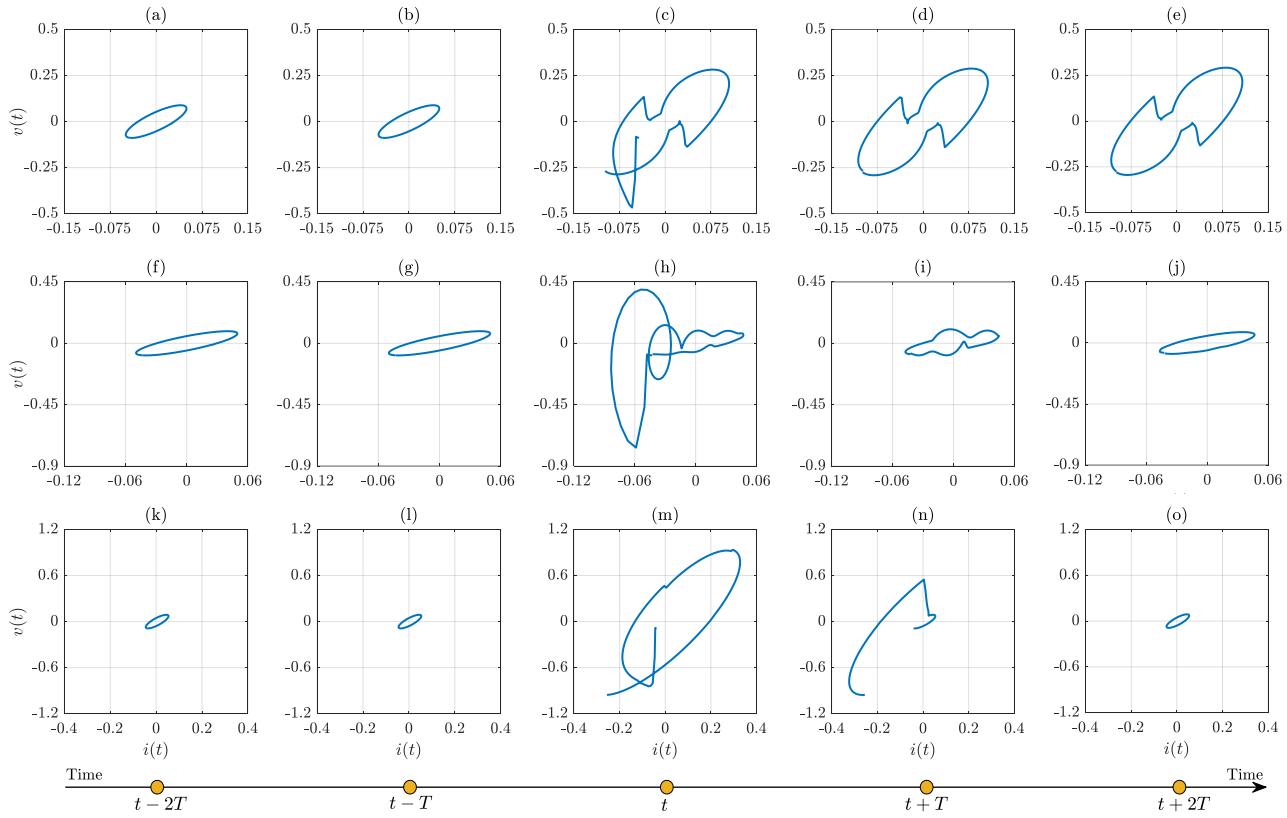

Fig. 3. Five cycles of synchronized Lissajous curves for three different types of events: (a)-(e) high impedance fault which is a sustained event; (f)-(j) capacitor bank switching which is a sustained event with a major transient component; (k)-(o) incipient fault which is only a short temporary event. T is one cycle period.

(1) and the current waveform in (2) for the purpose of obtaining the synchronized Lissajous curve. To see this, again consider the power distribution feeder with two WMUs that we saw in Fig. 1. Suppose an event occurs somewhere between the two WMUs. Once the event occurs, almost the entire event current flows through the substation at the upstream of the event, as opposed to flowing through the loads at the downstream of the event bus. This physical concept is commonly used in the literature in power distribution systems, e.g., see [12]; and it can be explained by comparing the Thevenin equivalent of the circuit at the upstream of the event with the Thevenin equivalent of the circuit at the downstream of the event. In particular, since the Thevenin impedance of the substation at the upstream of the event is much smaller than the Thevenin impedance of the loads at the downstream of the event, the event current is approximately equal to the change in the waveform $i_1(t)-i_2(t)$ that is defined in (2), i.e., the change in the difference between the current waveform that is measured at WMU 1 and the current waveform that is measured at WMU 2. As a result, the waveform in (2) provides valuable information about the current characteristics of the event.

We can similarly explain the physical intuition for the definition of the waveform in (1). Given the fact that the event current does not flow through the loads at the downstream of the event, it does *not* cause any change in the voltage at the buses at the downstream of the event. However, since the event current flows through the substation at the upstream of the event, it *does* cause some changes in the voltage at the buses at the upstream of the event. As a result, the change in voltage that is caused at the location of the event, which we can refer to as the event voltage, is approximately equal to the change in the waveform $v_1(t)-v_2(t)$ that is defined in (1), i.e., the change in the difference between the voltage waveform that is measured at WMU 1 and the voltage waveform that is measured at WMU 2. As a result, the waveform in (1) provides valuable information about the voltage characteristics of the event.

Accordingly, the synchronized Lissajous curve that is obtained by plotting the waveform in (1) versus the waveform in (2) can capture both the voltage characteristics and the current characteristics of the event, despite the fact that WMU 1 and WMU 2 are not at the location of the event; as the event rather occurs at an arbitrary location between WMU 1 and WMU 2.

Of course, an event may affect the characteristics of the voltage, the characteristics of the current, or the characteristics of both the voltage and the current. Thus, the synchronized Lissajous curve can be used to study different types of events. For example, a high impedance fault mostly affects the current waveform; as we saw in the synchronized Lissajous curve in Fig. 3(c); a capacitor bank switching mostly affects the voltage waveform; as we saw in the synchronized Lissajous curve in Fig. 3(h); and an incipient fault affects both the current waveform and the voltage waveform; as we saw in the synchronized Lissajous curve in Fig. 3(m).

III. Event Detection Method

Motivated by the examples and the analysis in Section II, our goal in this section is to use the synchronized Lissajous curves as the means to *detect* power quality events.

A. Similarity Index

Let us define the area of the synchronized Lissajous curve at time t over period T of the past cycle as follows:

$$Area(t) = \left| \int_{i(\tau=t-T)}^{i(\tau=t)} v(\tau)\, di(\tau) \right|. \tag{3}$$

During normal operating conditions, there is little to no difference between two successive calculations of the areas in (3). However, once an event occurs, such difference suddenly becomes significant. This can help us detect the event. Suppose $Area(t)$ and $Area(t-\Delta t)$ denote the areas of the synchronized Lissajous curves at times t and $t-\Delta t$, where Δt is the reporting interval of the WMUs, e.g., $\Delta t = 65$ μsec. We define the *similarity index* at time t as

$$\mathcal{S}(t) = 1 - \left| \frac{Area(t) - Area(t-\Delta t)}{max\big\{ Area(t), Area(t-\Delta t) \big\}} \right|. \tag{4}$$

If the areas of the two successive synchronized Lissajous curves are almost equal, then $\mathcal{S}(t)$ is close to one. However, if the areas of the two successive synchronized Lissajous curves are considerably different, then $\mathcal{S}(t)$ is close to zero, indicating that a sudden change has occurred in the synchronized Lissajous curve at time t. This means an event has occurred at time t.

B. Adaptive Detection Threshold

We propose an *adaptive* detection threshold by considering the past similarity indices to minimize the number of false alarms. In this regard, consider a window of time period W immediately before time t, i.e., from time $t-W$ to time $t-\Delta t$. The similarity indices of such window of duration W are

$$\mathcal{S}(t-W),\, \mathcal{S}(t-W+\Delta t), \cdots,\, \mathcal{S}(t-\Delta t). \tag{5}$$

Let us define $M(t)$ and $MAD(t)$ as the *median* and *median absolute deviation* of the similarity indices in (5) [32]. We propose to define the adaptive threshold as follows:

$$\mathcal{T}(t) = \alpha \Big(M(t) - \eta\, MAD(t) \Big), \tag{6}$$

where α is a number between 0 and 1 to control the sensitivity of the event detection method. A common choice for η is 2.5 [32]. We use the median and median absolute deviation statistics because they are robust against outliers. We detect an event at time t if the following inequality holds:

$$\mathcal{S}(t) < \mathcal{T}(t). \tag{7}$$

Importantly, the detection threshold must be revised after an event is detected. We *discard* the very small similarity index at event time from the next calculation of the adaptive threshold. That is, the similarity index at time t is used in the calculation of the next threshold *only if* time t is not an event time.

IV. Event Classification Method

Once the power quality event is detected by the proposed method in Section III, we construct a new synchronized Lissajous curve from the moment that the event is detected and for the duration of one cycle. Next, we need to identify the *type* of the detected power quality event based on this one-cycle synchronized Lissajous curve. Therefore, in this section, we propose a novel method based on *image classification* to categorize each detected event into different classes based on the shape of their one-cycle synchronized Lissajous curves.

First, we will discuss the factors that affect the shape of the synchronized Lissajous curves and why they make the classification problem a highly challenging task. Second, we will convert the detected synchronized Lissajous curves to images so that they can be classified by using image processing techniques. Third, we will develop an efficient Convolution Neural Network (CNN) to extract features of the synchronized Lissajous images in order to conduct event classification.

A. Challenging Factors

The shape of the synchronized Lissajous curve depends on not only the type (i.e., the class) of the event, but also other factors such as the angle, the location, and the size of the affected physical components. Therefore, even when we look at *different examples of the exact same class of events*, the shapes of the synchronized Lissajous curves can have considerable differences based on the above various factors. They can make the event classification problem challenging, as we explain next.

Impact of the Event Angle: Consider the synchronized Lissajous curves in Fig. 4. They both represent *the exact same disturbance*, which is a capacitor bank switching event. However, the firing angle of the switching action is different in these two cases. One switching event occurs near the positive peak of the voltage waveform. The other switching event occurs near the negative peak of the voltage waveform. We can see that the oscillations in the corresponding Lissajous curves start at two different places on the voltage-current plane; making the two curves look differently. In fact, one curve is almost the mirror reflection of the other curve. Therefore, we can conclude that the angle of the event can affect the shape of the synchronized Lissajous curve, thereby creating additional challenges and complications in the event classification problem.

Impact of the Event Location: Next, consider the synchronized Lissajous curves in Fig. 5. They represent *the exact same disturbance*, which is a high impedance fault with equal fault impedance. However, the location of the fault is different in these two cases; one is closer to the substation at the beginning of the feeder; while the other one is closer to the end of the feeder. We can see that the shapes of the two curves are somewhat similar; however, there are major *rotational differences* among these curves. If the fault occurs near the beginning of the feeder, i.e., near WMU 1, then the angle between the voltage difference waveform and the current difference waveform in the synchronized Lissajous curve is *smaller*, see Fig. 5(a). However, if the fault occurs near the

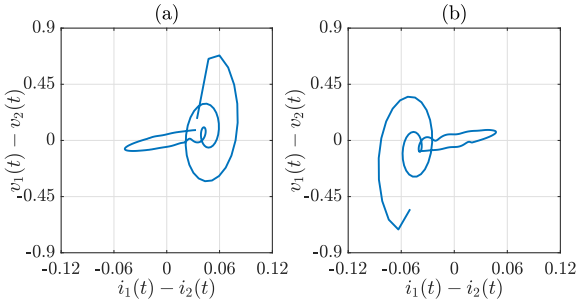

Fig. 4. The synchronized Lissajous curves during the same event that occurs at two different firing angle: (a) near positive peak; (b) near negative peak.

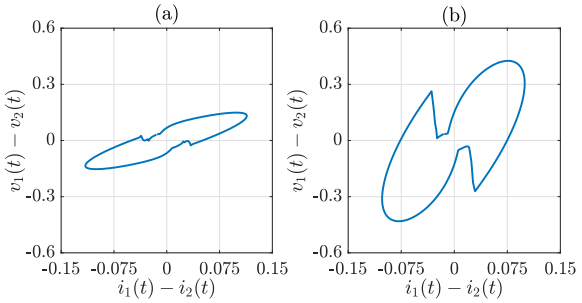

Fig. 5. The synchronized Lissajous curves during the same event that occurs at two different locations: (a) near WMU 1; (b) near WMU 2.

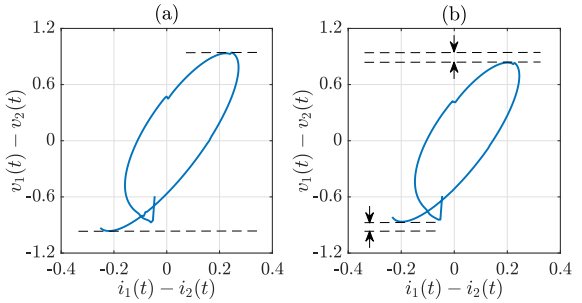

Fig. 6. The synchronized Lissajous curves during two incipient faults with different fault parameters: (a) lower fault impedance; (b) higher fault impedance.

end of the feeder, i.e., near WMU 2, then the angle between the voltage difference waveform and the current difference waveform in the synchronized Lissajous curve is *larger*, see Fig. 5(b). We can conclude that the location of the event can directly affect the shape of the synchronized Lissajous curve, thereby making classification a challenging task.

Impact of other Event Parameters: Finally, consider the synchronized Lissajous curves in Fig. 6. They show *the exact same disturbance*, which is an incipient fault. However, the impedance of the fault is different in these two cases. One fault has a smaller impedance. The other fault has a larger impedance. We can see that the shapes of the two curves are almost similar; however, the sizes of the curves are different; which is due to the different fault impedances. If the impedance of the incipient fault is smaller, then the size of the Lissajous curve is larger, see Fig. 6(a). Conversely, if the impedance of the incipient fault is larger, then the size of its corresponding Lissajous curve is smaller, see Fig. 6(b). We can conclude that the parameters of an event can highly affect not only the shape but also the size of the synchronized Lissajous curve.

B. Synchronized Lissajous Curve as Image

The challenges in Section IV-A can be addressed if we treat the synchronized Lissajous curves as *images* and subsequently take advantage of the recent advancements in the field of image processing to solve the event classification problem.

There are multiple reasons why it is beneficial to study a synchronized Lissajous curve as an *image*, as opposed to studying the raw synchronized waveform measurements as *time series*. *First*, graphical images can capture the overall *patterns* in the shape of the synchronized Lissajous curves; while such overall patterns are inherently spreed over time in the original time series. For example, there are clear similarities between the two synchronized Lissajous curves in Fig. 5. It is clear that one image is almost a *squeezed version* of the other image. Therefore, the two Lissajous images belong to the same class of events. However, such similarity would not be clear if we only look at the raw waveform measurements corresponding to these two events. *Second*, the sequential nature of time series is embedded with many important characteristics, which lays outside of a typical time-domain analysis. Therefore, it is difficult to perform classification in time-domain using the state-of-the-art sequence classification methods. *Third*, deep machine learning methods have shown particularly promising results in recent years in solving image processing problems. Therefore, if we present the event classification problem based on synchronized Lissajous curves as an image processing problem, then we benefit from powerful image processing tools.

The synchronized Lissajous curves are converted to synchronized Lissajous images by using various readily available conversion functions in MATLAB and/or Python. For example, one option is to use the combination of functions `getframe` and `frame2im` in MATLAB; see [33], [34].

We will verify the importance of treating synchronized Lissajous curves as images through case studies in Section V-C.

C. Convolutional Neural Networks

Once the synchronized Lissajous curves are converted to images, one can use various advanced image processing methods to classify the events based on their synchronized Lissajous images. In this paper, we use Convolutional Neural Networks (CNNs) to classify the detected Lissajous images into multiple classes of events. CNNs are effective deep machine learning techniques that are widely used in image recognition and speech recognition, among other fields [35], [36].

The structure of CNN includes an input layer, a few hidden layers, and an output layer. The input layer takes as input the synchronized Lissajous images of the detected power quality events. The hidden layers consist of the convolutional, batch normalization, activation, max-pooling, dropout, and the fully-connected layers. The convolutional layer is the key layer to extract features. It includes a series of kernel filters. The batch normalization layer normalizes the input, to speed up the training of the CNN. The activation layer implements non-linearity functions to the CNN model, by using functions such as sigmoid, hyperbolic tangent, or rectified linear unit (ReLU). The max-pooling layer performs down-sampling to summarize

TABLE I
THE STRUCTURE OF THE PROPOSED CNN MODEL

Layer	Layer Type	Activation
1.1	Convolutional	(120,120,60)
1.2	Batch Normalization	(120,120,60)
1.3	ReLU	(120,120,60)
2.1	Convolutional	(120,120,60)
2.2	Batch Normalization	(120,120,60)
2.3	ReLU	(120,120,60)
3.4	Max-Pooling	(60,60,60)
3.1	Convolutional	(60,60,120)
3.2	Batch Normalization	(60,60,120)
3.3	ReLU	(60,60,120)
3.4	Max-Pooling	(30,30,120)
3.5	Dropout	(30,30,120)
4.1	Fully-connected	(1,1,3)
4.2	Softmax	(1,1,3)
4.3	Classification	–

the extracted features. The dropout layer randomly assigns zero to the input to prevent over-fitting. The fully-connected layer integrates the features from the previous layers to the softmax activation layer to obtain probabilities of the input. The output layer is the classification layer that determines the label of the input image given the probabilities from the previous layer.

Table I shows the structure of the proposed CNN for event classification based on Lissajous images. It consists of a four-layer architecture, where each architecture includes multiple layers. Since the size of the input Lissajous images is large, a wide kernel filter is used in the first convolutional layer to extract more features from the Lissajous images. The ReLU is used in the activation layers to speed up learning and improve its performance [37]. Softmax is used in the final activation layer to get a probability distribution density for the classes. The proposed CNN classification approach is implemented in MATLAB using its available CNN model [38].

After examining a few different CNN structures, the current structure based on the four-layer CNN was selected due to its desirable performance. This structure is similar to the structure of other CNN-based image classification method in the literature, e.g. see [25]–[28]. The performance of the proposed classification method is examined in Section V-B and VI-B.

It bears mentioning that the size of a synchronized Lissajous image depends on the size of the event. This may affect the results in the classification task. This issue is addressed by *normalizing* each synchronized Lissajous curve with respect to its energy *before* the curves are converted to graphical images.

V. CASE STUDIES

In this section, we assess the performance of the proposed event detection and event classification methods. All simulations are done in PSCAD [39] based on the IEEE 33-bus test system. The one line diagram of the simulated test system is shown in Fig. 7. Two WMUs are assumed to be installed in the network. WMU 1 is installed at bus 1. WMU 2 is installed at bus 18. Each WMU captures the time-synchronized voltage and current waveforms at its location. To emulate real-world WMU measurements, white Gaussian noise is added to the simulated voltage and current waveform measurements. Unless stated otherwise, we consider a signal-to-noise-ratio (SNR) of 80 dB in both voltage and current waveforms. The nominal system frequency is 60 Hz. Unless stated otherwise, the reporting rate of the WMUs is assumed to be 256 samples per cycle.

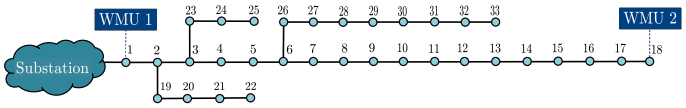

Fig. 7. The IEEE 33-bus distribution system with two WMUs.

The events that we study in this section are of the type that would typically require examining waveform measurements, i.e., they typically *cannot* be investigated properly by using phasor measurements. For example, we do not consider voltage sags, voltage swells, and interruptions; because they often do not require examining the waveform measurements in order to be detected or even classified. We also consider some events that *could* be captured by phasor measurements; but they are understood much better if one can instead capture the waveform measurements. One such example is capacitor bank switching; where capturing the waveform can further reveal the ringing oscillations as well as potential incipient faults.

The proposed event detection and event classification methods can be used both in post-mortem analysis and in real-time analysis. When it comes to real-time analysis, the steps that are taken are as follows. The proposed event detection method is run continuously to plot and examine the synchronized Lissajous curves to immediately detect any event as soon as it occurs. Once an event is detected, a new synchronized Lissajous curve of the detected event is plotted from the start time of the event and for a duration of one cycle. Most power quality events have a short duration, such as less than one cycle. Even for longer events, the event signature during the first cycle is particularly informative. Thus, one cycle of the synchronized Lissajous curve is long enough to examine the signature of a power quality event quickly after it is detected. This one-cycle synchronized Lissajous curve is then converted to a synchronized Lissajous image using an image conversion function, as it was previously explained in Section IV-B. Finally, the obtained synchronized Lissajous image is used as input to the proposed CNNs, which is already trained when it comes to real-time operation, in order to identify the type of the detected event.

A. Event Detection Results

We examine the performance of the proposed event detection method on three different classes of disturbances. Here, the sensitivity factor is set to 0.9; and the window duration is set to $W = 133$ msec. The results of event detection for the first class, i.e., the high impedance fault, the second class, i.e., the capacitor bank switching, and the third class, i.e., the incipient fault, are shown in Figs. 8(a), (b), and (c), respectively.

In Fig. 8(a), the similarity index drops from almost 1 to 0.82 at time $t = 0.50$ sec, indicating that an event occurs at this time, which is the correct event time. The similarity index fluctuates right after the event occurs, for about one cycle, from $t = 0.50$

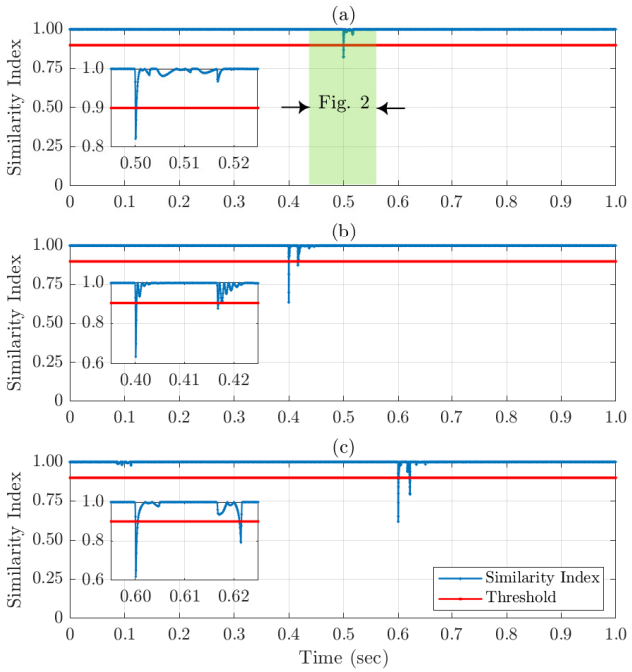

Fig. 8. The results for event detection, including the similarity index and the adaptive threshold for three example events: (a) the high impedance fault that we saw in Fig. 2; (b) a capacitor bank switching; (c) a sub-cycle incipient fault.

sec to $t = 0.517$ sec, see the zoomed-in figure. The similarity index goes back to almost 1 after time $t = 0.517$ sec. We can conclude that the event at time $t = 0.50$ sec is the only event that occurs during this one second period; and the event is a sustained event. Thus, the *profile* of the similarity index can help us identify the start time and the end time of each event. These are all useful parameters. For example, when it comes to event classification, the synchronized Lissajous curve from the start time of the event and for the duration of one cycle will be converted into an image. For the example in Fig. 8(a), we convert the synchronized Lissajous curve from time $t = 0.50$ sec to time $t = 0.517$ sec to an image. The image will be later used for event classification.

In Fig. 8(b), the similarity index drops from about 1 to nearly 0.6 at time $t = 0.40$ sec, indicating that an event occurs at this time; which is correct. One cycle later, the similarity index again drops from almost 1 to about 0.9 at time $t = 0.417$ sec, which is lower than the event detection threshold at this time. However, the similarity index rises to almost 1 after time $t = 0.417$ sec. Thus, the *profile* of the similarity index can help characterize the transient component of the event. It starts at time $t = 0.40$ sec and lasts for about one cycle till $t = 0.417$ sec. This is correct because the capacitor bank switching has a very short transient behaviour. We use the information on the similarity index profile to identify the correct duration of the event signature. In this example, we convert the synchronized Lissajous curve from time $t = 0.40$ sec to time $t = 0.417$ sec to an image. The image will be later used for event classification.

Finally, in Fig. 8(c), the profile of the similarity index indicates that an event occurs at time $t = 0.60$ sec, which is correct because the incipient fault is a temporary event that occurs for a short period of time. Hence, the results in Fig. 8(c) confirm the effectiveness of the proposed event detection method, even for events with very short duration. In this example, we convert the synchronized Lissajous curve from $t = 0.60$ sec till $t = 0.617$ sec to a synchronized Lissajous image. The image will be later used for event classification.

The above results confirms the effectiveness and the precision of the proposed power quality event detection method.

It bears mentioning that, the similarly index is obtained in an online setting, meaning that we obtain a new similarity index as soon as a new sample becomes available in the waveform measurements. This allows us to immediately detect an event and analyze it as soon as it happens. The computation time of the proposed event detection method is less than 0.3 msec; therefore, it can be used for real-time event detection.

B. Event Classification Results

In this section, we assess the performance of the proposed event classification method. We first generate a database for the synchronized voltage and current waveforms from two WMUs that occur during 120 events. For each event, we capture one second (60 cycles) of voltage and current waveforms at each WMU. Thus, we collect four synchronized waveforms for each event over 60 cycles. The data for each event includes a few cycles before the event and a few cycles after the event. Each event generates $4 \times 60 \times 256 = 61,440$ samples of data. We generate one synchronized Lissajous image for each event. Thus, the number of synchronized Lissajous images is 120 images. The size for input images of the CNN model is 240×240. The database consists of 40 high impedance faults, 40 capacitor bank switching, and 40 incipient faults with short arcs, where they are labeled in the following three classes of disturbances: Class I for high impedance faults, Class II for capacitor bank switching, and Class III for incipient faults.

The database is divided into three data sets: training data, validation data, and test data. The training data set includes 70% of the total events which are selected randomly. The validation data set includes 10% of the total events. The test data set includes the remaining 20% of the total events. We use Adam optimization algorithm to train the CNN model, see [40]. The initial learning rate in the training process is set to 1×10^{-4}, which remains constant throughout the training. The maximum number of epochs is set to 100, with the mini-batch size of 32.

The training accuracy of the proposed classification method converges to 100% and the validation accuracy converges to 97%; the figures are not shown here. The small difference between the two accuracies indicates the generalization capability of the proposed classification method to unseen events.

The confusion matrix for the *test* results for the proposed Lissajous-based CNN model is shown in Fig. 9(a). The diagonal entries denote the events that are classified *correctly*. The off-diagonal entries denote the events that are classified *incorrectly*. For each class, the accuracy is at least 91.7%. High impedance faults (Class I) and incipient faults (Class III) are classified better than capacitor bank switching (Class II). The minor shortcoming in the classification of capacitor bank

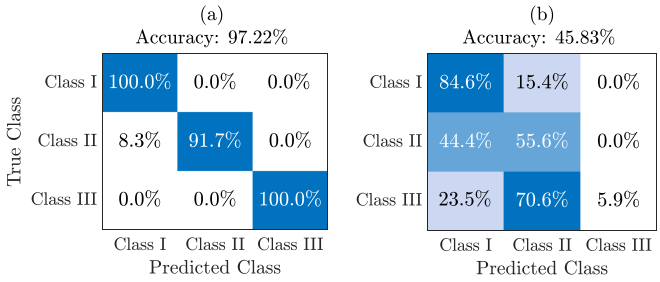

Fig. 9. Confusion matrix for the test data when we use: (a) the proposed CNN-based image classification method; (b) the competing RNN-based classification method that uses the raw time series measurements.

TABLE II
PERFORMANCE METRICS CORRESPONDING TO THE CONFUSION MATRIX IN FIG. 9(A)

Class	Precision	Sensitivity	Specificity	F_1 Score
I	100.0%	92.3%	100.0%	96.0%
II	100.0%	100.0%	100.0%	100.0%
III	94.4%	100.0%	96.8%	97.1%

switching is because the image of a capacitor bank switching has some features that also exist in other events. Interestingly, the converse is not true and all the incipient faults are classified correctly. The overall accuracy of the test results is 97.2%, which is close to the accuracy of the training results, i.e. 100%.

Next, we use the following various statistical metrics to further evaluate the performance of the proposed classification method: precision, sensitivity (a.k.a. recall), specificity, and F_1 score. Table II shows each metric for each class. As we can see, the worst-case precision and the worst-case specificity rates of the proposed classification method are 94.4% and 96.8%, respectively, both for Class III (incipient faults). Also, the worse-case sensitivity and the worst-case F_1 score rates are 92.3% and 96.0%, respectively, both for Class I (high impedance faults). These additional metrics further confirm the performance of the proposed event classification method.

Fig. 10 shows the Receiver Operating Characteristic (ROC) curve of the proposed event classifier at each class. The Area Under Curve (AUC) for each class is marked in the legend box. The ROC curve is a graph that shows the classifier's ability to distinguish different classes for different probability thresholds. It is obtained by plotting the sensitivity versus the $1-$specificity at different threshold settings. As we can see in Fig. 10, the AUC is at least 0.971, which indicates that the proposed event classifier can almost perfectly distinguish classes from each other. These results reveal the high performance of the proposed event classification model in correctly classifying events.

C. Classification based on Images versus Time Series

As we discussed in Section IV, it is highly beneficial to do event classification based on the synchronized Lissajous *images*, as opposed to based on the raw synchronized waveform measurements in time domain. This point is verified here by comparing the proposed CNN classification method that uses synchronized Lissajous images with a recurrent neural network

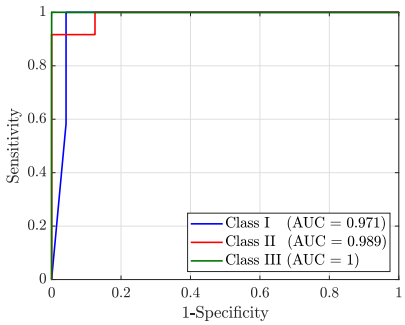

Fig. 10. The ROC curve of the proposed event classifier at each class. The AUC corresponding to each class is marked inside the legend box. Notice that the ROC curve for Class III appears on the x-axis and the y-axis.

(RNN) classification method that uses the time series of voltage and current waveforms. The latter method is implemented by developing a long short-term memory (LSTM) network to classify the time series of voltage difference waveform in (1) and the current difference waveform in (2). An LSTM is an RNN that takes time series as input. The hidden layers include two LSTM layers, a dropout layer, a fully connected layer, and a softmax layer. The output layer is the classification layer.

To have a fair comparison, we apply the RNN classification method and our proposed classification method to the *same* training data set and the *same* test data set.

The confusion matrix for the *test* results of the time series classification model is shown in Fig. 9(b). The overall accuracy is 45.83%, which is much smaller than the overall accuracy of our Lissajous-based classification method, i.e., 97.2%.

The above results verify the effectiveness of the proposed classification method based on Lissajous images.

From the above results, there are indeed advantages to conduct event classification by using the synchronized Lissajous curves, as opposed to using the raw time-series. The key advantage here is the fact that synchronized Lissajous images can better capture the *fundamental similarities* between the events of the *same type*; that we may sometimes miss if we solely look at the raw measurements as time-series. For example, the *same type* of event may create some characteristics in the raw synchronized waveform measurements that can vary depending on the location of the event or the size of the event. Such variations can sometimes make it difficult for the classification algorithms to realize the fact that the events belong to the *same type*, if we examine the raw measurements as time-series, see [9]. Thus, when possible, it is recommended to use the synchronized Lissajous curves for event classification.

D. Sensitivity Analysis

First, we investigate the impact of the reporting rate of the WMUs on the performance of the proposed event classification method. We consider four different reporting rates: 32, 64, 128, and 256 samples per cycle. In all four cases, we reach 100% accuracy for the training data. The accuracy for the test data varies between 95.8% at 32 samples per cycle to 97.2% at

256 samples per cycle. This confirms the effectiveness of the proposed method even at lower measurement reporting rates.

Next, we examine the performance of the proposed event classification method against measurement noise. We consider three different noise levels: 40 dB (very noisy), 60 dB (noisy), and 80 dB (less noisy). The results reveal that the accuracy always reaches 100% for the training data and it is at least 97.2% for the test data. This confirms the robustness of the proposed method even under significant noise levels.

Next, we study the performance of the proposed event classification method against missing data. We assume that we momentarily lose a chunk of measurements; which means we need to construct the synchronized Lissajous curve with missing measurements. We consider three different sizes for the window of data that is missed: 5%, 10% and 15%. The results reveal that the accuracy for the test data varies between 97.2% under 5% missing data to 94.4% under 15% missing data. This further confirms the robustness of the proposed method even under low reliability conditions of the waveform measurements.

E. Performance Comparison

In this section, we compare the performance of the proposed event classification method with the comparable state-of-the-art method in [28]. Importantly, both the method in this paper and the method in [28] conduct event classification by using image processing based on CNN. However, the method in [28] does *not* use synchronized Lissajous curves. Instead, it uses a graphical method that is based on the *space-phasor model* (SPM). The purpose of the method in [28] is to characterize voltage waveforms from one WMU to identify the type of events. In the context of the analysis in this paper, the method in [28] makes use of the waveform measurements from WMU 1, i.e., the WMU that is located at the upstream of the event. This method does *not* use the synchronized measurements from WMU 2. Thus, similar to most methods in the literature, the method in [28] is inherently *not* designed to take advantage of the synchro-waveforms from multiple WMUs. SPM is a *complex number* and it is calculated as follows [28]:

$$\text{SPM}(t) = \frac{2}{3}\left(v_1^A(t) + \alpha v_1^B(t) + \alpha^2 v_1^C(t)\right), \qquad (8)$$

where $\alpha = e^{\text{j}2\pi/3}$ and $\text{j} = \sqrt{-1}$. The superscripts denote the phase. That is, $v_1^A(t)$, $v_1^B(t)$, and $v_1^C(t)$ denote the voltage waveform measurements at WMU 1 on Phase A, Phase B, and Phase C, respectively. The SPM *image* is then generated by plotting the *imaginary* part of $\text{SPM}(t)$ over the *real* part of $\text{SPM}(t)$. The method in [28] applies the CNN-based image classification approach to the SPM images.

To have a fair comparison, we apply the classification method in [28] as well as our proposed classification method to the same database. The dataset in this case study is three-phase; otherwise the SPM formulation in (8) cannot be used. For our method, we use the synchronized Lissajous image based on one phase only, i.e., one of the phases that is affected by the event.

Fig. 11 shows the confusion matrix when we apply the method in [28] to the test data. As we can see, the overall accuracy is 75%, which is not bad, but considerably less than the overall accuracy of our Lissajous-based classification method at 97%, see Fig. 9(a). There are at least two reasons for the better performance of the proposed event classification method. One reason comes from the fact that SPM is not a suitable formulation to represent events that are almost balanced on all three phases. Notice that, by construction, SPM is identical (in form of a circle) for all balanced events. Thus, in general, the use of SPM is only suitable when the focus is on distinguishing balanced events versus unbalanced events. When it comes to distinguishing different types of balanced events, the method in [28] cannot differentiate the events because of their very similar shapes in the SPM images.

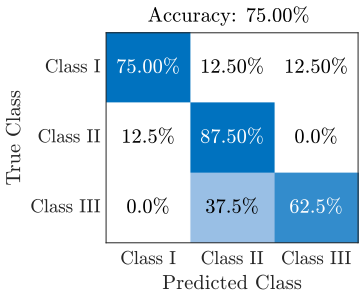

Fig. 11. Confusion matrix for applying the method in [28]. The results can be compared with those in Fig. 9(a).

Another reason for the better performance of the proposed method is that it uses *both* voltage waveforms and current waveforms. This is an inherent property of the Lissajous graph. There would be no synchronized Lissajous curve without using the synchronized current measurements. However, the method in [28] does not use the current waveform measurements.

In summary, the use of the proposed synchronized Lissajous images has fundamental advantages over the use of SPM images; even though both method ultimately involve image processing for the purpose of event classification.

VI. Experimental Results

While the case studies in Section V were extensive and insightful, they were all based on computer simulations. To complement the results in Section V, in this section, we provide additional case studies that are based on *experimental* results.

A. Real-World Field Measurements

In this section, we evaluate the performance of the proposed event detection method by using real-world synchro-waveform measurements from the publically available data set on the EPRI/DoE (Electric Power Research Institute/Department of Energy) website [41]. This data set contains three-phase voltage waveform and three-phase current waveforms for about 300 power quality disturbances. The waveforms are recorded using various power quality sensors, therefore, they have different reporting rate, ranging from 16 samples per cycle up to 128 samples per cycle. Importantly, the vast majority of the waveform measurements in the EPRI/DoE data set are *not*

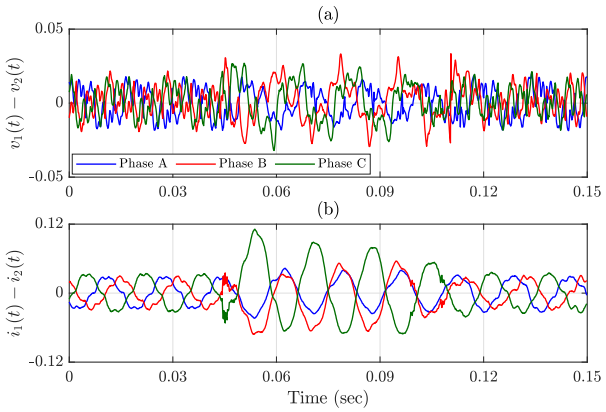

Fig. 12. An example for real-world synchronized waveform measurements during an event: (a) three-phase voltage difference waveform; (b) three-phase current difference waveform. The two sets of three-phase waveforms are from the waveform records 2892 and 2893 in the EPRI/DoE database [41].

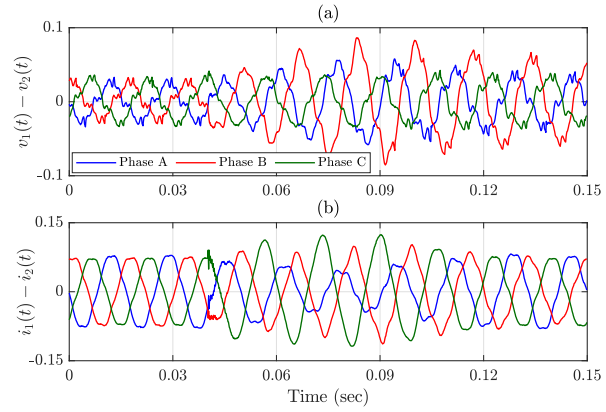

Fig. 13. Another example for real-world synchronized waveform measurements during an event: (a) three-phase voltage difference waveform; (b) three-phase current difference waveform. The two sets of three-phase waveforms are from the waveform records 2787 and 2786 in the EPRI/DoE database [41].

synchro-waveforms; they are rather individual unsynchronized waveform measurements. However, there *are* very few cases where *synchronized* waveform measurements were obtained by two waveform sensors for the *same* event.

We use two examples of such real-world synchro-waveform measurements. The first example includes the synchronized measurements from two WMUs at Record Numbers 2892 and 2893. This event is related to a line tripping that happened during a lightning. The second example includes the synchronized measurements from two WMUs at Record Numbers 2786 and 2787. This event is related to a fault that happened during a major storm. As the starting point for our analysis, we used the above raw waveform measurements and obtained the *difference waveforms* as in (1) and (2). Given that the measurements in [41] are three-phase, we obtained the difference waveforms for each phase. Figs. 12 and 13 show the obtained difference waveforms in the first example and the second example, respectively.

1) Performance of Event Detection: Figs. 14(a) and (b) show the profile of the similarity index for the real-world synchronized waveform measurements in Figs. 12 and 13,

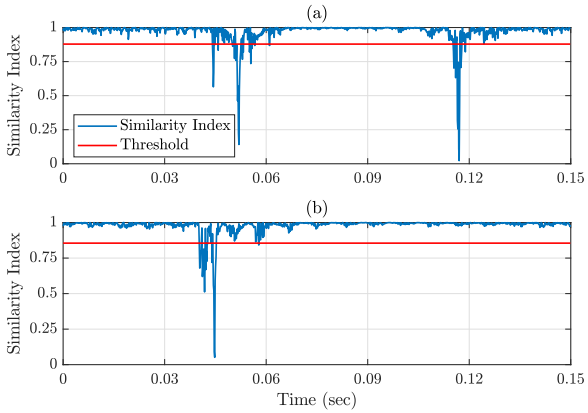

Fig. 14. The results of event detection applied to the real-world synchronized waveform measurements, including the similarity index and the adaptive threshold: (a) Phase B of the difference waveform measurements in Fig. 12; (b) Phase C of the difference waveform measurements in Fig. 13.

respectively. Only one phase is shown here. The similarity index profile in Fig. 14(a) indicates that the event occurs at time $t = 0.045$ sec, which is indeed correct. The similarity index then fluctuates right after the event for about five cycles, from $t = 0.045$ sec to $t = 0.12$ sec. The similarity index goes back to almost 1 after time $t = 0.12$ sec. The similarity index profile in Fig. 14(b) indicates that an event occurs at time $t = 0.04$ sec, which is correct. Hence, the results in Figs. 14(a) and (b) further confirm the accuracy of the proposed event detection method, including for real-world waveform measurements.

2) Comparison with Another Graphical Tool: Next, we compare the proposed method that is based on using synchronized Lissajous curves with another graphical method that was proposed in [28]. The graphical method in [28] is based on the SPM from one WMU, as we discussed in Section V-E.

From (8), it is clear that the method in [28] does *not* use the current waveforms, as opposed to the method in this paper that uses *both* voltage and current waveforms. This limitation was *not* an issue in [28]; because the primary purpose of the study in [28] was to classify events based on whether they involve disturbances on *one phase*, on *two phases*, or on *three phases*. Because of such focus on the analysis of unbalance, the method in [28] did not need to reveal all the characteristics of the event on each phase. However, this is needed for the type of study that is done in this paper, i.e., to examine the detailed shape of the event on every phase, even in a single-phase system. Clearly, if we focus on one phase only, the method in [28] is no longer applicable; because SPM is all about the *relative* shape of the voltage waveforms across the three phases.

Figs. 15 and 16 show nine successive cycles of the synchronized Lissajous images and the SPM images corresponding to the real-world event in Fig. 12. As we can see, the shape of the SPM image in the nine cycles in Fig. 16 are more or less the same, making it difficult to identify the detailed characteristics of the event. However, the synchronized Lissajous images in Fig. 15 do take *very different shapes* when the event occurs, e.g., see the image at cycle 4 in Fig. 15(d), and compare it with the image at cycle 3 in Fig. 15(c) and the image at cycle 7 in

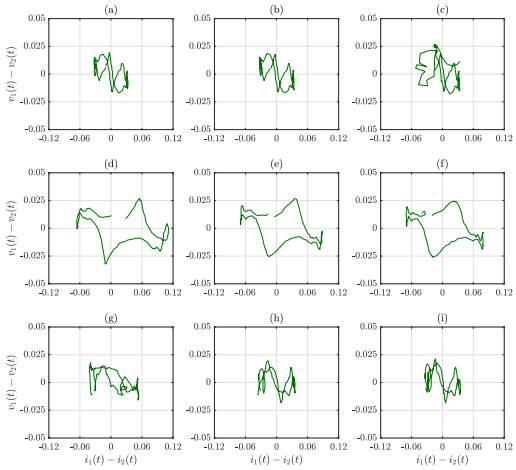

Fig. 15. Nine cycles of the synchronized Lissajous curves on Phase C for the real-world waveform event in Fig. 12.

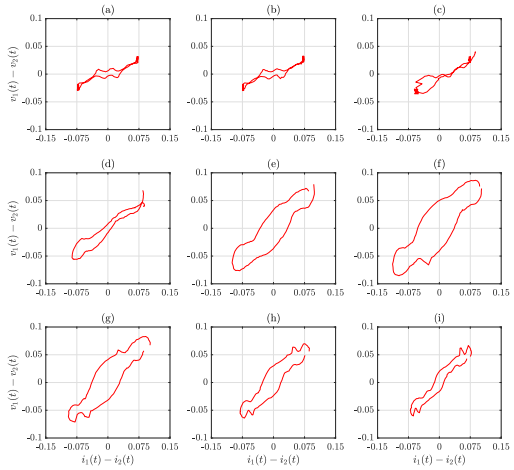

Fig. 17. Nine cycles of the synchronized Lissajous curves on Phase C for the real-world waveform event in Fig. 13.

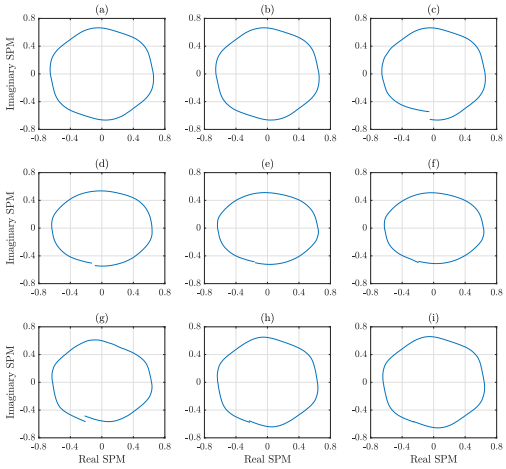

Fig. 16. Nine cycles of the SPM curves [28] for the same real-world waveform event that was discussed in Fig. 12. Compare the graphs with those in Fig. 15.

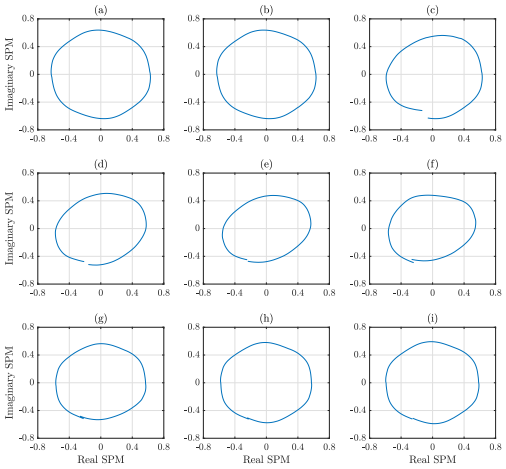

Fig. 18. Nine cycles of the SPM curves [28] for the same real-world waveform event that was discussed in Fig. 13. Compare the graphs with those in Fig. 17.

Fig. 15(g), i.e., before and after the event. Notice that the new shape of the synchronized Lissajous curve remains for a total of about three cycles, from cycle 4 to cycle 6, see Figs. 15(d)-(f). Thus, the synchronized Lissajous images draw a unique and more comprehensive picture about the presence and the characteristics of the event, much more than the SPM images.

Therefore, although both the synchronized Lissajous images and SPM images are regular images, the shape of the synchronized Lissajous images provide us with further, and more insightful information about the characteristics of the event.

We can make similar observations also for the second example of the real-world synchronized waveform measurements in Fig. 13. Figs. 17 and 18 show nine successive cycles of the synchronized Lissajous images and SPM images corresponding to this example. Comparing the images in Figs. 17 and 18, we can again see that the synchronized Lissajous images provide more information and *more distinction* about the event, compared to the SPM images. This further confirms the effectiveness of the proposed graphical tool for event monitoring.

B. Hardware-in-the-Loop Testing

The real-world field measurements in Section VI-A were suitable for the analysis of the proposed event detection method. They were also useful to highlight the importance of using the proposed synchronized Lissajous curve, compared to other graphical tools in the literature, such as in [28]. However, such real-world field measurements are not sufficient to train and to test the proposed event classification method. Therefore, in this section, we conduct Hardware-in-the-Loop (HIL) testing so that we can examine the event classification method.

HIL testing is a technique for testing an external hardware in real-time simulations. For the purpose of this study, we used HIL testing to capture real-time waveform measurements by using an *external hardware* for the sensor device. Our HIL testing setup consists of the following components, as shown in Fig. 19: 1) a Real Time Digital Simulator (RTDS) that simulates a power distribution network in real-time [42]. Importantly, RTDS is the industry standard HIL testing equipment that is widely used by utilities; 2) a multi-channel BK Precision

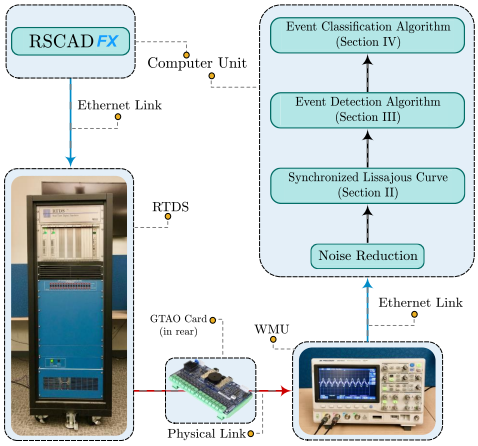

Fig. 19. The architecture of the implemented HIL testing experiments.

2569 Series Digital Storage and Mixed Signal Oscilloscope that serves as the external WMU hardware; 3) a computer unit that runs the simulations and also receives and stores the real-time measurements; 4) the RSCAD software that is used for running the simulations on the RTDS [43]; and 5) the algorithmic software that we developed in MATLAB to collect the raw waveform measurements from the external WMU hardware, conduct noise reduction, obtain the synchronized Lissajous curves, obtain the corresponding images, and conduct event classification according to the proposed graphical method.

The power distribution network that is simulated in RSCAD inside the RTDS is the same IEEE 33-bus distribution feeder that we previously saw in Fig. 7. The voltage waveform and the current waveform from bus 1 and bus 18 are extracted from RTDS to feed into the ports of a GTAO (GIGA-Transceiver Analog Output) Card to generate external Analog waveforms. Such Analog waveforms are then supplied as inputs to the channels of the external WMU hardware. The differential synchro-waveforms are then captured by the external WMU hardware and subsequently sent to a computer server through an Ethernet connection, i.e., a Local Area Network (LAN) cable. The obtained measurements are then used to evaluate the performance of our proposed event classification methods.

The distribution of different classes, the assumptions, and the choices of the training parameters remain the same as in Section V-B. Since the waveform measurements are done by using an actual external hardware sensor, the raw measurements are *noisy*. Thus, before we can use the waveform measurements, we need to do *noise reduction*. We do so by using a lowpass filter to remove the high frequency noises from the raw measurements.

Figs. 20(a) and (b) show the confusion matrix for the test data, without and with initial noise reduction, respectively. As we can see, the proposed model is able to correctly classify most of the unseen events in the HIL tests. The overall accuracy of the test results is 88.9% for the case without initial noise reduction, see Fig. 20(a), and 94.4% for the case with initial noise reduction, see Fig. 20(b). The results further confirm the effectiveness of the proposed event classification method.

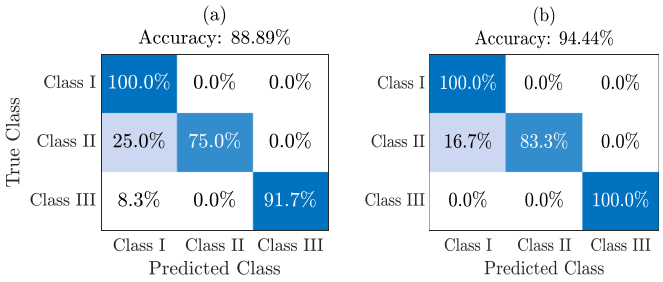

Fig. 20. Confusion matrix for applying the proposed event classification method to the test data in HIL testing: (a) without initial noise reduction; (b) with initial noise reduction.

VII. Discussions on Real-Life Applications and Future Works

While the focus in this paper is on the core technical tasks of event detection and event classification in synchro-waveform measurements, the results can ultimately support different real-life applications. Some of these potential applications as well as a few directions for future works are discussed in this section.

First, the methodologies that are developed in this paper can help improve situational awareness with respect to the state of *health* and *safety* of various equipment in power distribution systems. In particular, by detecting and identifying incipient faults, the utility can take remedial actions in a timely manner to prevent catastrophic damages in the future, i.e., to resolve a major future failure while it is still in its early stages. Of course, since incipient faults are usually self-clearing and last for only a very short period of time [3], [12], improving our ability to detect and classify incipient faults can directly benefit the ultimate real-life applications in this area.

Second, detection and identification of specific equipment operations, such as switching on and switching off at capacitor banks, can also help with scrutinizing the operation of certain equipment of interest. This can benefit us with not only identifying any potential malfunctions but also updating the utility models to keep track of the changes in the system due to equipment aging [2]. The latter results can help improve the overall operation of the power distribution system.

Finally, as for the real-life applications of detecting and identifying high impedance faults, and even some incipient faults, they can be used for instance in wildfire detection and prevention [44]. Note that, a high impedance fault occurs when a line conductor touches a high grounding impedance object, such as during vegetation intrusion or when the power line is down. These circumstances can cause ignition and ultimately lead to wildfire [45]. In fact, many of the most destructive wildfires in California are reported to be caused by power equipment issues, see [46]. Hence, early detection and identification of high impedance faults can contribute to improving our ability to detect and prevent wildfires.

The analysis in this paper can be extended in various directions. In fact, we believe that the proposed synchronized Lissajous curves can be insightful even beyond event detection and event classification. For example, one option for future work is to examine the synchronized Lissajous curves

to identify the location of events, specially during transient events and incipient faults. Another potential extension is to examine multi-dimensional images; which can be constructed to using synchronized waveform measurements from several sensors. Other extensions could include applying other methods in image processing to conduct event classification based on synchronized Lissajous images; such as the methods that are used in optical character recognition in computer vision. Last but not least, while we did apply our proposed event detection method to a number of representative real-world synchronized waveform measurements, more testing can be done in practice.

VIII. Conclusions

A new data-driven situational awareness framework is proposed in power distribution systems based on the analysis of synchro-waveform measurements. Such measurements are provided by waveform measurement units, which are an emerging class of smart grid sensors. The new framework is built upon a fundamentally new concept, called the synchronized Lissajous curve, where we plot the difference of two synchronized voltage waveforms versus the difference of two synchronized current waveforms. The synchronized Lissajous curves provide insight about the operation of the power system during power quality events, thereby improving our knowledge about the root cause and the characteristics of various events. We used the changes in areas of two successive synchronized Lissajous curve as the metric to detect an event. The proposed detection method is able to accurately detect events and also identify the start time and the end time of each event. We also used the images of the synchronized Lissajous curves to classify the detected events. In this regard, we developed a CNN-based image classification method. The proposed classification method is able to classify power quality events with high accuracy, even at very low measurement reporting rate, under missing data, and under very noisy environment. Furthermore, some real-life applications and potential future works are discussed.

References

[1] A. F. Bastos, S. Santoso, W. Freitas, and W. Xu, "Synchrowaveform measurement units and applications," in *Proc. IEEE PES General Meeting*, Atlanta, GA, USA, 2019, pp. 1–5.

[2] M. Izadi and H. Mohsenian-Rad, "Event location identification in distribution networks using waveform measurement units," in *Proc. IEEE PES ISGT Europe*, the Hague, Netherlands, 2020, pp. 924–928.

[3] M. Izadi and H. Mohsenian-Rad, "Synchronous waveform measurements to locate transient events and incipient faults in power distribution networks," *IEEE Trans. Smart Grid*, vol. 12, no. 5, pp. 4295–4307, Sep. 2021.

[4] [Online]. Available: https://selinc.com

[5] [Online]. Available: https://www.candura.com

[6] [Online]. Available: https://www.sentient-energy.com

[7] I. Niazazari, H. Livani, A. Ghasemkhani, Y. Liu, and L. Yang, "Event cause analysis in distribution networks using synchro waveform measurements," in *Proc. North American Power Symposium*, Tempe, AZ, USA, 2021, pp. 1–5.

[8] M. Izadi and H. Mohsenian-Rad, "A synchronized Lissajous-based approach to achieve situational awareness using synchronized waveform measurements," in *Proc. IEEE PES General Meeting*, Washington, DC, 2021, pp. 1–5.

[9] M. Izadi and H. Mohsenian-Rad, "Characterizing synchronized lissajous curves to scrutinize power distribution synchro-waveform measurements," *IEEE Trans. Power Syst.*, vol. 36, no. 5, pp. 4880–4883, Sep. 2021.

[10] H. Mohsenian-Rad, E. Stewart, and E. Cortez, "Distribution synchrophasors: pairing big data with analytics to create actionable information," *IEEE Power Energy Mag.*, vol. 16, no. 3, pp. 26–34, May 2018.

[11] W. Xu, Z. Huang, X. Xie, and C. Li, "Synchronized waveforms – a frontier of data-based power system and apparatus monitoring, protection, and control," *IEEE Trans. Power Deli.*, vol. 37, no. 1, pp. 3–17, Feb. 2022.

[12] H. Mohsenian-Rad, *Smart Grid Sensors: Principles and Applications*. Cambridge University Press, Cambridge, UK, 2022.

[13] [Online]. Available: https://www.wecc.org/Administrative/GE-WAMS-Sub-Synchronous%20Oscillations%20-%20March%202020.pdf

[14] G. Zweigle, "Monitoring point-on-wave measurements from a wide area," in Panel Session on synchronized waveform measurements: technology, requirements and applications, *IEEE Power and Energy Society General Meeting*, 2021.

[15] B. Gao, R. Torquato, W. Xu, and W. Freitas, "Waveform-based method for fast and accurate identification of subsynchronous resonance events," *IEEE Trans. Power Syst.*, vol. 34, no. 5, pp. 3626–3636, Sep. 2019.

[16] D. Macii and D. Petri, "Rapid voltage change detection: Limits of the IEC standard approach and possible solutions," *IEEE Trans. Instrnm. Meas.*, vol. 69, no. 2, pp. 382–392, Feb. 2020.

[17] W. Gao and J. Ning, "Wavelet-based disturbance analysis for power system wide-area monitoring," *IEEE Trans. Smart Grid*, vol. 2, no. 1, pp. 121–130, Mar. 2011.

[18] S. M. A. Bhuiyan, J. Khan, and G. Murphy, "WPD for detecting disturbances in presence of noise in smart grid for PQ monitoring," *IEEE Trans. Ind. Appl.*, vol. 54, no. 1, pp. 702–711, Jan.-Feb. 2018.

[19] P. K. Ray, N. Kishor, and S. R. Mohanty, "Islanding and power quality disturbance detection in grid-connected hybrid power system using wavelet and S-transform," *IEEE Trans. Smart Grid*, vol. 3, no. 3, pp. 1082–1094, Sep. 2012.

[20] S. Santoso, W. M. Grady, E. J. Powers, J. Lamoree, and S. C. Bhatt, "Characterization of distribution power quality events with Fourier and wavelet transforms," *IEEE Trans. Power Deli.*, vol. 15, no. 1, pp. 247–254, Jan. 2000.

[21] P. D. Achlerkar, S. R. Samantaray, and M. Sabarimalai Manikandan, "Variational mode decomposition and decision tree based detection and classification of power quality disturbances in grid-connected distributed generation system," *IEEE Trans. Smart Grid*, vol. 9, no. 4, pp. 3122–3132, Jul. 2018.

[22] S. Mishra, C. N. Bhende, and B. K. Panigrahi, "Detection and classification of power quality disturbances using S-transform and probabilistic neural network," *IEEE Trans. Power Deli.*, vol. 23, no. 1, pp. 280–287, Jan. 2008.

[23] Z. Liu, Y. Cui, and W. Li, "A classification method for complex power quality disturbances using EEMD and rank wavelet SVM," *IEEE Trans. Smart Grid*, vol. 6, no. 4, pp. 1678–1685, Jul. 2015.

[24] A. J. Wilson, D. R. Reising, R. W. Hay, R. C. Johnson, A. A. Karrar, and T. Daniel Loveless, "Automated identification of electrical disturbance waveforms within an operational smart power grid," *IEEE Trans. Smart Grid*, vol. 11, no. 5, pp. 4380–4389, Sep. 2020.

[25] S. Ekici, F. Ucar, B. Dandil, and R. Arghandeh, "Power quality event classification using optimized bayesian convolutional neural networks," *Electr. Eng.*, vol. 103, p. 67–77, Feb. 2021.

[26] S. K. G. Manikonda, S. Gangwani, S. P. K. Sreckala, J. Santhosh, and D. N. Gaonkar, "Power quality event classification using convolutional neural networks on images," in *Proc. IEEE Int' Conf. Energy Syst. Inf. Process. (ICESIP)*, Chennai, India, 2019, pp. 1–5.

[27] S. Wang and P. Dehghanian, "On the use of artificial intelligence for high impedance fault detection and electrical safety," *IEEE Trans. Ind Appl.*, vol. 56, no. 6, pp. 7208–7216, Nov.-Dec. 2020.

[28] A. Bagheri, I. Y. H. Gu, M. H. J. Bollen, and E. Balouji, "A robust transform-domain deep convolutional network for voltage dip classification," *IEEE Trans. Power Deli.*, vol. 33, no. 6, pp. 2794–2802, Dec. 2018.

[29] D. Karacor, S. Nazlibilek, M. H. Sazli, and E. S. Akarsu, "Discrete Lissajous figures and applications," *IEEE Trans. Instrum. Meas.*, vol. 63, no. 12, pp. 2963–2972, Dec. 2014.

[30] T. Hong and F. de León, "Lissajous curve methods for the identification of nonlinear circuits: calculation of a physical consistent reactive power," *IEEE Trans. Circuits Syst. I, Reg. Papers*, vol. 62, no. 12, pp. 2874–2885, Dec. 2015.

[31] A. Abu-Siada and S. Mir, "A new on-line technique to identify fault location within long transmission lines," *Engineering Failure Analysis*, vol. 105, pp. 52–64, Nov. 2019.

[32] C. Leys, C. Ley, O. Klein, P. Bernard, and L. Licata, "Detecting outliers: Do not use standard deviation around the mean, use absolute deviation

around the median," *Journal of Experimental Social Psychology*, vol. 49, no. 4, pp. 764–766, Jul. 2013.
[33] MathWorks. Matlab Help Center - Getframe. [Online]. Available: https://www.mathworks.com/help/matlab/ref/getframe.html
[34] MathWorks. Matlab Help Center - Frame2im. [Online]. Available: https://www.mathworks.com/help/matlab/ref/frame2im.html
[35] K. Simonyan and A. Zisserman, "Very deep convolutional networks for large-scale image recognition," *arXiv preprint arXiv:1409.1556*, 2015.
[36] A. Krizhevsky, I. Sutskever, and G. E. Hinton, "ImageNet classification with deep convolutional neural networks," in *Proc. Advances Neural Inf. Process. Syst.*, vol. 25, 2012, p. 1097–1105.
[37] V. Nair and G. E. Hinton, "Rectified linear units improve restricted boltzmann machines," in *Proc. Int' Conf. Mach Learn.*, Haifa, Israel, 2010, pp. 807–814.
[38] [Online]. Available: https://www.mathworks.com/discovery/convolutional-neural-network-matlab
[39] Manitoba HVDC Research Centre. ver. 4.2 PSCAD/EMTDC (Software Package), Winnipeg, MB, Canada.
[40] D. P. Kingma and J. Ba, "Adam: A method for stochastic optimization," *arXiv preprint arXiv:1412.6980*, 2014.
[41] EPRI/DOE National Database Repository of Power System Events. [Online]. Available: http://pqmon.epri.com
[42] Real Time Digital Simulator (RTDS). [Online]. Available: http://www.rtds.com
[43] Real Time Digital Simulator Tutorial Manual. ver. RSCAD FX (Software Package), Winnipeg, MB, Canada..
[44] S. Jazebi, F. de León, and A. Nelson, "Review of wildfire management techniques—part I: causes, prevention, detection, suppression, and data analytics," *IEEE Trans. Power Deli.*, vol. 35, no. 1, pp. 430–439, Feb. 2020.
[45] J. A. Wischkaemper, C. L. Benner, B. Don Russell, and K. Muthu Manivannan, "Application of advanced electrical waveform monitoring and analytics for reduction of wildfire risk," in *Proc. IEEE PES ISGT*, Washington, DC, 2014, pp. 1–5.
[46] Top 20 most destructive California wildfires, *California Department of Forestry and Fire Protection,* Sacramento, CA, USA, 2021. [Online]. Available: https://www.fire.ca.gov

Milad Izadi (S'17) received the B.Sc. degree in electrical engineering from Razi University, Kermanshah, Iran, in 2015, the M.Sc. degree in electrical engineering from Sharif University of Technology, Tehran, Iran, in 2017. He is currently a Ph.D. student in electrical engineering and a Bonnie Reiss Carbon Neutrality Initiative Fellow at the University of California, Riverside, CA, USA. He is interested in the intersection of data analysis, machine learning, optimization, and simulation in power system applications. He is the pioneer on the analysis and applications of *synchronized waveform measurements* in power systems. He is specifically working on applications of *waveform measurement units* (WMUs) and phasor measurement units (PMUs) in power distribution systems. He was the 2019 Best Reviewer of the IEEE TRANSACTIONS ON SMART GRID and was the recipient of the 2019 Best Master Thesis Award from the Smart Grid Conference in Iran.

Hamed Mohsenian-Rad (M'09-SM'14-F'20) received the Ph.D. degree in electrical and computer engineering from the University of British Columbia, Vancouver, BC, Canada, in 2008. He is currently a Professor of electrical engineering and a Bourns Family Faculty Fellow at the University of California, Riverside, CA, USA. His research is on monitoring, data analysis, and optimization of power systems and smart grids. He is the author of the textbook *Smart Grid Sensors: Principles and Applications* by Cambridge University Press - 2022. He was the recipient of the National Science Foundation (NSF) CAREER Award, the Best Paper Award from the IEEE Power & Energy Society General Meeting, and the Best Paper Award from the IEEE Conference on Smart Grid Communications. He has been the PI on ten million dollars research grants in the area of smart grid. He has served as Editor for the IEEE TRANSACTIONS ON POWER SYSTEMS, IEEE TRANSACTIONS ON SMART GRID and the IEEE POWER ENGINEERING LETTERS.